ORIGINAL PAPER

THE USE OF LA-ICP-MS AS AN AUXILIARY TOOL TO ASSESS THE PULMONARY TOXICITY OF MOLYBDENUM(IV) SULFIDE (MoS$_2$) NANO- AND MICROPARTICLES

RENATA KURAŚ[1], MACIEJ STĘPNIK[2,3], KATARZYNA DOMERADZKA-GAJDA[2], and BEATA JANASIK[4]

[1] Nofer Institute of Occupational Medicine, Łódź, Poland
Central Laboratory

[2] Nofer Institute of Occupational Medicine, Łódź, Poland
Department of Toxicology and Carcinogenesis

[3] QSAR LAB Ltd., Gdańsk, Poland

[4] Nofer Institute of Occupational Medicine, Łódź, Poland
Department of Chemical Safety

Abstract

Objectives: Laser ablation inductively coupled plasma mass spectrometry (LA-ICP-MS) has considerable applicative potential for both qualitative and quantitative analyses of elemental spatial distribution and concentration. It provides high resolutions at pg-level detection limits. These qualities make it very useful for analyzing biological samples. The present study responds to the growing demand for adequate analytical methods which would allow to assess the distribution of nanostructured molybdenum(IV) disulfide (MoS$_2$) in organs. It was also motivated by an apparent lack of literature on the biological effects of MoS$_2$ in living organisms. The study was aimed at using LA-ICP-MS for comparing micro- and nanosized MoS$_2$ ditribution in selected rat tissue samples (lung, liver, brain and spleen tissues) after the intratracheal instillation (7 administrations) of MoS$_2$ nano- and microparticles vs. controls. **Material and Methods:** The experimental study, approved by the Ethics Committee for Animal Experiments was performed using albino Wistar rats. This was performed at 2-week intervals at a dose of 5 mg/kg b.w., followed by an analysis after 90 days of exposure. The MoS$_2$ levels in control tissues were determined with the laser ablation system at optimized operating conditions. The parameter optimization process for the LA system was conducted using The National Institute of Standards and Technology (NIST) glass standard reference materials. **Results:** Instrument parameters were optimized. The study found that molybdenum (Mo) levels in the lungs of microparticle-exposed rats were higher compared to nanoparticle-exposed rats. The opposite results were found for liver and spleen tissues. Brain Mo concentrations were below the detection limit. **Conclusions:** The LA-ICP-MS technique may be used as an important tool for visualizing the distribution of Mo on the surface of soft samples through quantitative and qualitative elemental mapping. Int J Occup Med Environ Health. 2024;37(1):18–33

Key words:
microparticles, LA-ICP-MS, molybdenum(IV) disulfide, bioimaging, rat tissues, nanoparticles

INTRODUCTION

Laser ablation combined with inductively coupled plasma mass spectrometry (LA-ICP-MS) is an analytical technique employed to ionize samples. It is highly sensitive and does not require a mineralization step or a preliminary preparation of solutions. It has undergone rapid developments in the past few decades and become useful for various fields of science. Its main use has been for the assessment of the distribution and accumulation of trace elements and toxic metals in biomedical samples, including clinical ones [1–4]. Data on the spatial distribution of toxic and vital elements in tissues help to explore and understand bodily processes. However, there continues to be insufficient research on the optimization of analytical procedures for the determination of nanoparticle (NP) concentrations in soft tissues using LA-ICP-MS [5,6].

Molybdenum (Mo) is a trace element forming part of the enzymes that catalyze many metabolic changes [7]. In a solid form, it is not significantly hazardous. When pulverized, it has flammable properties. In dust form, this element displays weakly sensitizing properties. There is uncertainty related to the safety of, and exposure to, Mo-NPs (molybdenum(IV) disulfide [MoS_2]) in manufacturing and work settings. This is because insufficient is known about the toxicity mechanism of Mo-NPs [8,9]. A recent report has indicated dose-dependent inflammatory changes in rat lungs after a single intratracheal administration of nano- and micro-sized MoS_2 [10]. The authors have found acute toxicological effects in male rats at a dose of 1.5 or 5 mg/kg b.w. Histopathological analysis revealed Mo microparticle deposition in respiratory tissues for up to 7 days. Furthermore, it has been reported that molybdenose may cause uric acid accumulation, which may then lead to gout, a decrease in bone mineral density – mainly due to disorders in steroid hormone concentrations – and impaired fertility [11–13]. Further data on Mo levels and distribution in animal tissues may, therefore, prove useful for assessing the poten-

tial toxicity of Mo-NPs. The authors assume that local variations in nano- and micromolecular Mo concentrations may play an important role here. A comparison of the distribution and accumulation of Mo in tissues of rats exposed to nano- and micro-sized Mo particles with control tissue sections will provide valuable information on the spatial distribution of Mo. It will be a very helpful tool to assess the activity of this element in nanoform and its possible health effects.

The study will further research on the potential short- and long-term toxic respiratory effects of MoS_2 and its tissue distribution. It will involve the bioimaging of tissues collected from animals (rats) exposed to MoS_2 and Mo in ionic form to assess MoS_2 toxicity. Moreover, soft tissue (brain, lung, liver, spleen) sections will be used to determine the distribution, location and concentration of both Mo forms with the LA-ICP-MS technique. Laser ablation microsampling will enable the visualization of tissue structures, providing an important tool to assess the potential harmful effects of exposure to Mo-NPs.

There is currently no research on the spatial distribution of nano- and micro-sized Mo particles in soft tissues of animals exposed to MoS_2. However, there have been experimental studies involving silver (Ag) and manganese (Mn) NPs [14–16] which suggest that tissue bioimaging could provide a valuable tool for the assessment of Mo nanoparticle toxicity.

MATERIAL AND METHODS
Reagents and standards

The parameter optimization process for the laser ablation (LA) system was conducted using The National Institute of Standards and Technology (NIST) Standard Reference Materials (SRM) glass standard materials (NIST610, NIST612, NIST614; NIST SRM, Gaithersburg, MD, USA). Subsequently, NIST SRM was applied as an internal quality control measure after assuring constant operating conditions.

Agarose gel standards were prepared by mixing 0.2 g of agarose powder (Sigma-Aldrich, Darmstadt, Germany) with appropriate dilutions of the stock solution (modified methods according to [16,17]). For all calibration procedures, standard solutions were prepared from 10.00±0.05 mg/l. Multi-Element Certified Reference Material (CRM) Comprehensive Mix B Standard (LGC, Manchester, NH, USA) by dilution with ultra-pure deionized water (Milli-Q Integral 3 system, Millipore, Bedford, MA, USA) (≤18.2 MΩ/cm) and 65% nitric acid (HNO_3) (ULTREX II Ultrapure Reagent, J.T. Baker™, Allentown, PA, USA). The Multi-Element CRM Comprehensive Mix B Standard was applied since the initial aim was to use carbon and sulfur as internal standard (IS) correction and also because other elements were measured in the same experiment. The calculated calibration ranges for Mo determination in pellet standards were 0.5–50 µg/l.

In order to validate the method, the dogfish liver CRM for Trace Metals and other Constituents (NRC-DOLT-5; NRC-CNRC, Ontario, Canada) was used to produce a powder tablet. Additional CRMs were tablets of mussel tissue (SRM 2976; NIST, Gaithersburg, MD, USA) and human hair (NCS DC 73347a; China National Analysis Center, Beijing, China). Approximately 200 mg of lyophilized material were loaded into a tablet press with a 13 mm diameter (Specac Atlas™ Manual 15T, Orpington, England) and pressed int o a tablet by applying 10 t (0.74 × 106 kPa) for 1 min. Argon (Ar) gas purity was >99.999%.

Preparation of MoS_2 colloid and suspension

Molybdenum(IV) disulfide colloid and suspension in water were prepared, with the addition of polyvinylpyrrolidone (at a mass ratio of MoS_2: PVP = 1:1, 10 000–200 000 Da, Sigma-Aldrich, Co. LLC, Sait Louis, MO, USA) as a stabilizer. A colloidal system with nanosized particles in the range of 50–100 nm, and a suspension containing microsized particles in the range of 0.5–5 µm were pre-

pared. Detailed information on the preparation of MoS_2 particles, their physico-chemical analysis using high-resolution scanning electron microscopy (SEM) and scanning transmission electron microscopy (STEM) microscopy, as well as on the dynamic light scattering (DLS) technique with zeta potential measurements, including the internalization of MoS_2 particles by STEM with energy-dispersive X-ray spectroscopy (EDS) analysis, can be found in Sobańska et al. [10].

Sample and slide preparation for LA-ICP-MS

The experimental study, approved by the Ethics Committee for Animal Experiments (Resolution No. 6/ŁB 86/2018), was performed using albino Wistar rats (age: 6–8 weeks, weight: 80–120 g). Tissues from at least 4 animals were selected for further assay according to OECD Guidelines for the Testing of Chemicals, Section 4 Test No. 417: Toxicokinetics (adopted on July 22, 2010). The volumes of the PVP solution and nano- and microsized MoS_2 suspensions to be instilled intratracheally were calculated individually for each animal. The proportions were maintained depending on body weight, at a dose of 1.5 mg or 5 mg MoS_2/kg b.w. The controls were administered with a corresponding dose of the PVP solution. Next, selected rats were dissected under anesthesia [10]. After macroscopic examinations and weighing procedures, all organs intended for LA-ICP-MS were formalin-fixed in 10% neutral buffered formalin and paraffin-embedded. Brain, spleen, lung and liver samples were embedded in paraffin (automated Belair RVG/1 Vacuum Tissue Processor, Rankin, Davisburg, MI, USA), and then in paraffin blocks (TES 99 Tissue Embedding System, Medite GmbH, Burgdorf, Germany). Subsequently, they were cut into 20 µm thick sections (HM 325 Rotary Microtome, MICROM International GmbH, Walldorf, Germany). A glass base slide was used, since glass does not generate a high background for the analyte to be investigated with the LA system. Moreover, the glass slides were coated with agarose to standardize the method.

The formalin and paraffin, as well as the PVP solution and agarose samples, were analyzed using ICP-MS to eliminate analyte contamination.

Instrumentation

The measurements were conducted using the LA system (J200 Tandem LA/LIBS Applied Spectra Inc., West Sacramento, USA) equipped with a high-energy laser (Nd:YAG) operating at a 266 nm wavelength, in which yttrium-aluminum garnet was the matrix ($Y_3Al_2(AlO_4)_3$), with an admixture of neodymium ions (Nd^{3+}), and combined with the ICP-MS detection system (Nexion, 350x, Perkin Elmer, SCIEX, Framingham, USA). The ICP-MS settings were tuned to obtain the minimum ceric oxide

ratio and the minimum doubly charged barium ion ratio, and maximum stable signal intensities of the NIST612 glass solid standard and selected tissue samples. Other instrumental parameters are summarized in Table 1. All optimized parameters were set to allow the ablation of the whole tissue.

The ICP-MS was triggered by laser during the analysis. The project applied the line-by-line mode. Applied Spectra, Inc.'s Data Analysis was employed to visualize signal intensity. Quantitative distribution in tissue sections was compared with sections obtained from controls.

RESULTS

Selection of Mo isotopes for the analysis

The signal intensity for Mo and the relative standard deviation (RSD) were observed as a relative change in the LA system's operating parameters. In this paper, the results concerned the ^{98}Mo isotope, which was selected according to the highest abundance, a better signal as well as a better signal-to-blank ratio, and a lower RSD, in comparison to other isotopes. However, all 7 stable Mo isotopes were checked, as shown in Table 2, along with selected potential interferences (especially isobars and oxide ions) to make adjustments if required ($-0.109613 \times {}^{101}$Ru).

Table 1. Main parameters of the instruments used for the study on distribution of nanostructured molybdenum(IV) disulfide (MoS$_2$) in organs of albino Wistar rats

Parameter	Value
Laser ablation system	
laser energy [mJ]	1.2–2.9
repetition frequency [Hz]	10
spot size [μm]	100
scan speed [μm/s]	100
carrier gas flow helium (He) [l/min]	0.7
make-up flow argon (Ar) [l/min]	0.7
Inductively coupled plasma mass spectrometry (ICP-MS)	
gas flow [l/min]	
nebulizer	1
auxiliary	1.2
plasma	18
RF power [W]	1450
dwell time per isotope [ms]	8
cones	Ni
detector mode	dual (pulse counting and analog mode)
measured isotopes	^{92}Mo, ^{94}Mo, ^{95}Mo, ^{96}Mo, ^{97}Mo, ^{98}Mo, ^{100}Mo, ^{13}C, ^{32}S

Table 2. Molybdenum isotopes and their potential interference forming in plasma (based on [18] and [19])

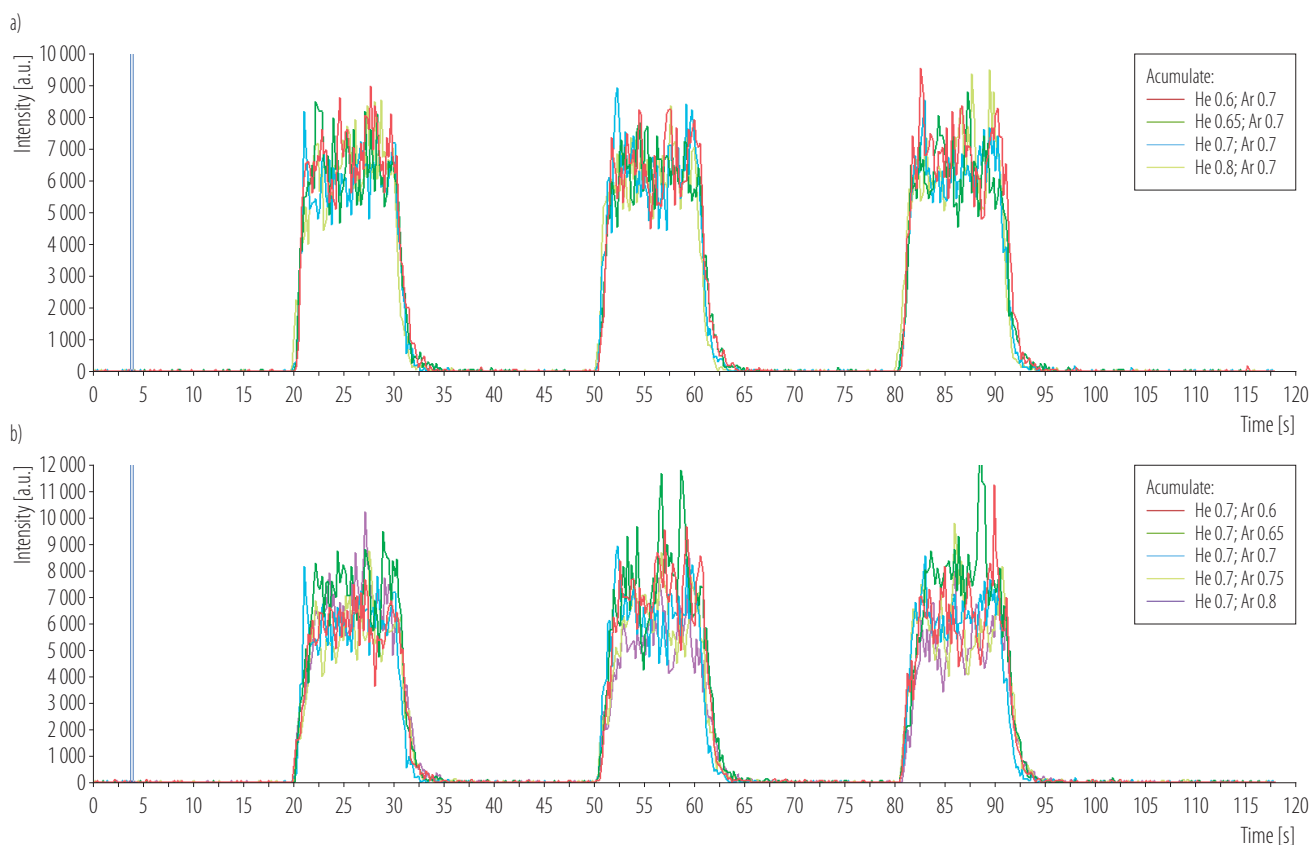| Molybdenum isotope	Relative natural abundance [%]	Potential interference
^{92}Mo	14.84	^{75}As^{17}O$^+$, ^{76}Se^{16}O$^+$, ^{92}Zr$^+$
^{94}Mo	9.25	^{78}Se^{16}O$^+$, ^{39}K$_2$^{16}O$^+$, ^{94}Zr$^+$
^{95}Mo	15.92	^{40}Ar^{39}K^{16}O$^+$, ^{78}Se^{16}OH$^+$, ^{79}Br^{16}O$^+$
^{96}Mo	16.68	^{80}Se^{16}O$^+$, ^{79}Br^{17}O$^+$, ^{96}Zr$^+$, ^{96}Ru$^+$
^{97}Mo	9.55	^{40}Ar$_2$^{16}O^{1}H$^+$, ^{40}Ca$_2$^{16}O^{1}H$^+$, ^{80}Se^{16}OH$^+$, ^{81}Br^{16}O$^+$, ^{40}Ar^{40}K^{16}O$^+$
^{98}Mo	24.13	^{82}Se^{16}O$^+$, ^{81}Br^{17}O$^+$, ^{41}K$_2$O$^+$, ^{98}Ru$^+$
^{100}Mo	9.63	^{84}Se^{16}O$^+$, ^{81}Br^{19}O$^+$, ^{100}Ru$^+$

Image from Applied Spectra's data analysis software, Aurora.

Figure 1. Selection of optimal gas flows for the laser ablation (LA) system: a) optimized helium (He) gas flow rate with a constant argon (Ar) flow rate (0.7 l/min), b) optimized Ar gas flow rate with a constant He flow rate (0.7 l/min) in the study on distribution of nanostructured molybdenum(IV) disulfide (MoS_2) in organs of albino Wistar rats

Selection of optimal gas flows for the LA system

When comparing the variable He gas flow rate (0.6 l/min, 0.65 l/min, 0.7 l/min, 0.8 l/min) at a constant Ar gas velocity (0.7 l/min) (Figure 1a) and the variable Ar gas flow rate (0.6 l/min, 0.65 l/min, 0.7 l/min, 0.75 l/min, 0.8 l/min) at a constant He gas velocity (0.7 l/min) (Figure 1b), larger deviations in signal intensity were observed at extreme flows. Accordingly, the most economical variant was chosen (0.7 Ar and 0.7 He l/min).

Optimization of laser beam energy

The maximum energy that can be obtained during the operation of an LA system is 100%, which corresponds to 24.1 mJ. The laser beam energy comparison was per-

formed in the range of 1–90% (Figure 2a), while the exact optimization was in the range of 1–10% (Figure 2b).

Optimization of repetition frequency

The study investigated the effect of pulse frequency in the range of 2–10 Hz on analyte signal intensity (Figure 2c). It can be seen that signal intensity increases and the RSD decreases as pulse duration length increases. Note that 10 Hz was taken as the optimal value, or the maximum value, for the J200 Tandem LA-LIBS.
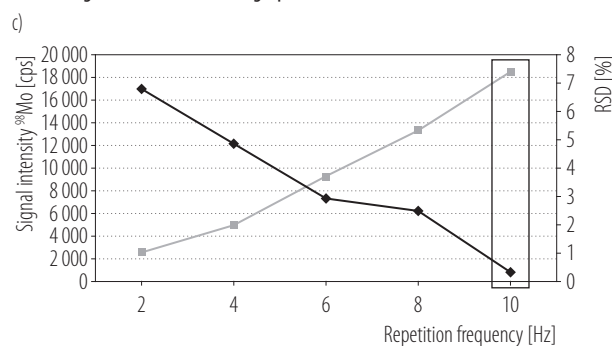
Optimization of scanning speed

The optimum scanning speed at the minimum RSD is 0.025 mm/s (Figure 2d).
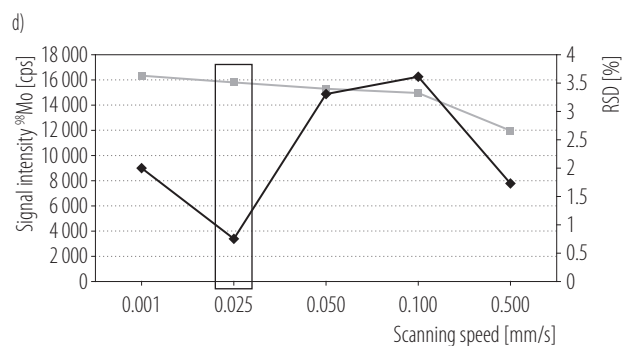
a)
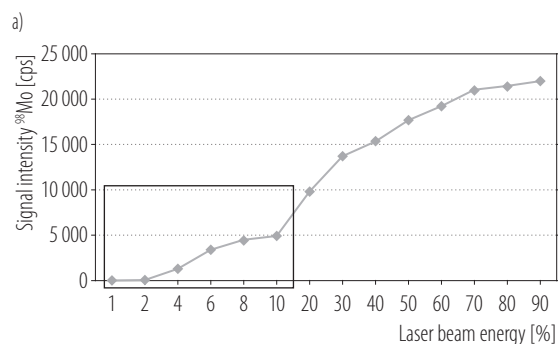
The rectangle is the exact optimization of laser beam energy
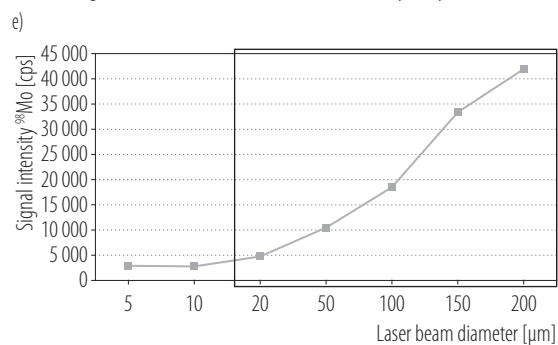in the range of 1–10% shown in graph b.
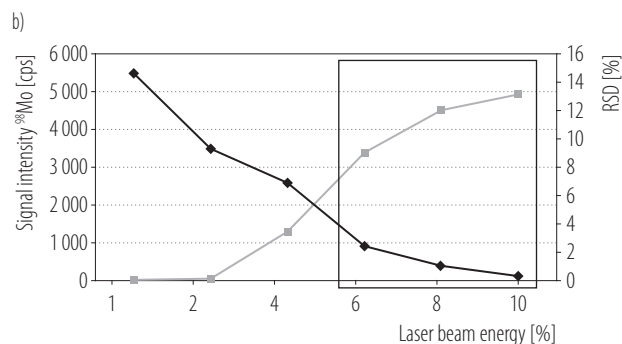
b)

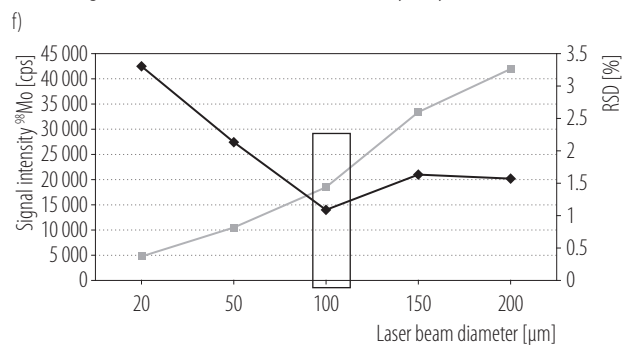The rectangle is the final result taken for further analysis by authors.

c)

The rectangle is the final result taken for further analysis by authors.

d)

The rectangle is the final result taken for further analysis by authors.

e)

The rectangle is the exact optimization of the laser beam diameter shown
for the 20–200 µm range in graph f.

f)

The rectangle is the final result taken for further analysis by authors.

Figure 2. Molybdenum isotope ^{98}Mo signal intensity as a function of the relative standard deviation (RSD %) and a) laser beam energy for the 1–90% range, b) laser beam energy for the 1–10% range, c) repetition frequency, d) scan speed, e) the laser beam diameter for the 5–200 µm range, and f) the laser beam diameter for the 20–200 µm range in the study on distribution of nanostructured molybdenum(IV) disulfide (MoS$_2$) in organs of albino Wistar rats

Laser beam diameter setting

Signal intensity at the collimated spot was very low (Figure 2e). This study was based on a spot diameter of 100 µm to reach a compromise between the smallest diameter, where the RSD value is low, and a high value of signal intensity (Figure 2f).

Selection of the operating mode

The effect of each mode is shown in Figure 3. For the standard mode, the chamber gas flow rate and the rejection parameter q (RPq) were not optimized because RPq was equal to 0.25 and there was no reaction/collision gas. The use of methane (CH₄) in the dynamic reaction
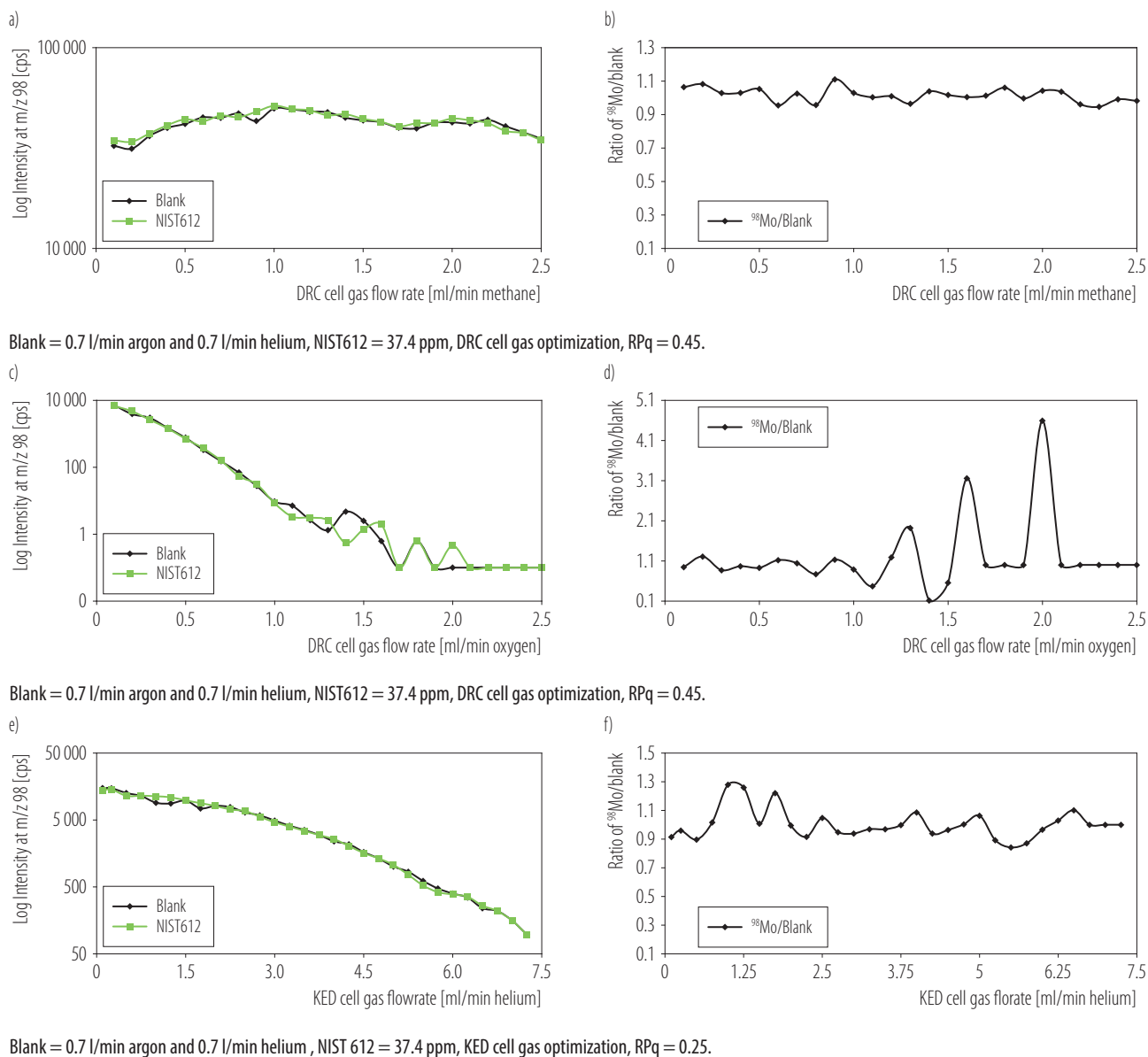
a)

b)

Blank = 0.7 l/min argon and 0.7 l/min helium, NIST612 = 37.4 ppm, DRC cell gas optimization, RPq = 0.45.

c)

d)

Blank = 0.7 l/min argon and 0.7 l/min helium, NIST612 = 37.4 ppm, DRC cell gas optimization, RPq = 0.45.

e)

f)

Blank = 0.7 l/min argon and 0.7 l/min helium , NIST 612 = 37.4 ppm, KED cell gas optimization, RPq = 0.25.

Figure 3. Effect of the a), b) methane flow rate in the dynamic reaction cell (DRC) mode; c), d) oxygen flow rate in the DRC mode; e), f) kinetic energy discrimination (KED) mode helium flow rate on Mo ion signal intensity at m/z 98 in the study on distribution of nanostructured molybdenum(IV) disulfide (MoS_2) in organs of albino Wistar rats

cell (DRC) chamber (Figure 3a and 3b) did not reveal any significant differences in signal intensity for Mo to the background, although compared to other analyzed gases (oxygen [O] and helium [He]), the signal intensity was significant. Interference removal by O in the DRC chamber (Figure 3c and 3d) probably generated molybdenum oxides or hydroxides simultaneously

($^{94}Mo^{16}OH^+/^{95}Mo^{16}O^+$), which in turn could be oxidized to higher oxides ($^{95}MoO^{2+}/^{95}MoO^{3+}$). Hence, higher ratios at single gas flows (1.3 ml/min, 1.6 ml/min, 2.0 ml/min) could only be an interference in the optimization process. It was experimentally verified that the selection of a different Mo isotope did not result in clear deviations from these interferences. The use of non-reactive He in
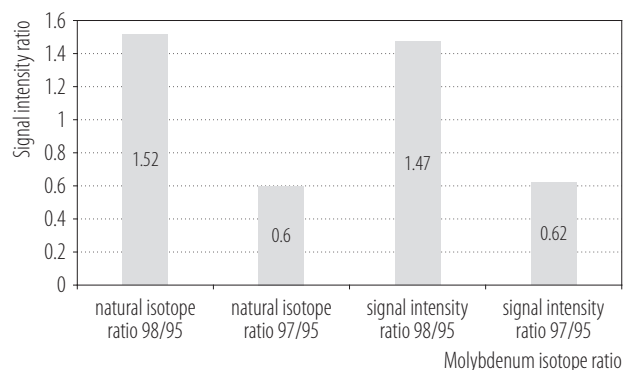
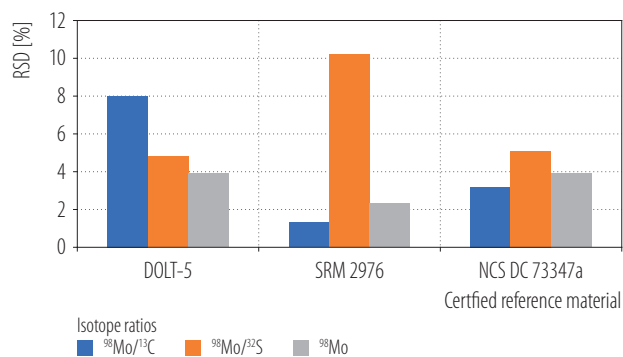Standard mode, 0.7 l/min argon and 0.7 l/min helium.

Figure 4. Isotopic analysis of National Institute of Standards and Technology (NIST612)

C – carbon; Mo – molybdenum; S – sulfur.
DOLT-5 – dogfish liver; NCS DC 73347a – human hair; SRM 2976 – 2977 mussel tissue.

Figure 5. Comparison of ^{98}Mo vs. internal standard (^{98}Mo/^{13}C and ^{98}Mo/^{32}S) for the 3 available certified reference material pellets (N = 4)

the ion discrimination chamber due to kinetic energy (Figure 3e and 3f) did not yield the desired difference in analytical signal intensity to background noise. After optimizing the operation of the spectrometer in DRC and in the kinetic energy discrimination (KED) modes, the standard mode without gas in the chamber was chosen for the analysis of the tissue sections.

In order to confirm the validity of the standard mode on ICP-MS, as well as to verify the stability of the apparatus for further analysis, signal intensity ratios of $^{98/95}$Mo and $^{97/95}$Mo were compared with the natural isotope ratio (Figure 4). Note that NIST612 was analyzed 5 times with coefficients of variation at 3.08%, 3.09% and 2.94% for ^{95}Mo, ^{97}Mo, and ^{98}Mo, respectively.

**Standard sample
and quality control preparation for Mo analysis**

Comparisons of the linear regression equation and regression coefficients, both without (^{98}Mo: y = 3527.6x – 1970.6; r = 0.9992) and with IS (^{98}Mo/^{13}C: y = 0.0109x – 0.0072; r = 0.9989), (^{98}Mo/^{32}S: y = 0.0546x – 0.0018; r = 0.9933), and their calculated precision of the calibration curve, amounted to 8.07%, 7.99%, and 22.01%, respectively. Calibration was performed 3 times and the results were given as a mean of 3 replicate ablation lines (ca. 0.5–1.0 cm long)

per gel. Finally, a calibration strategy without internal standardization was applied to ensure optimum precision in the range of 3.15–13.26%. The authors calculated the RSD for ^{98}Mo signal intensity without standardization and the obtained value was normalized to the signal of selected ^{13}C and ^{32}S as IS in the 3 available CRMs (Figure 5). The smallest fluctuations of the RSD were noticed without normalization, from 2.3% to 3.9% vs. ^{98}Mo/^{13}C from 1.3% to 8.0%. Since validation by multiple measurements of the NIST612 glass is known to be inappropriate due to matrix inconsistency, a homogeneous pellet of dogfish liver CRM (DOLT-5) was used to verify the aplied method. The target mean of Mo for DOLT-5 was 1.41 μg/g (SD = 0.22 μg/g) vs. estimated mean 1.28 μg/g (SD = 0.16 μg/g). To determine the repeatability/reproducibility of LA-ICP-MS analysis, the same determinations were repeated on the same day and on different days. Intra- and inter-assays assays of coefficients of variation and the analysis of recovery of Mo obtained from 8 replicate ablation lines (ca 1.5 cm long) per DOLT-5 pellet yielded the following results: 12.9%, 16.5% and 90%, respectively. The limit of detection (LOD: 3 × SD/slope) estimated by the repetitive analysis (N = 10) of the blank agarose sample was at 0.017 μg/g and the limit of quantitation (LOQ: 6 × SD/slope) was 0.034 μg/g.
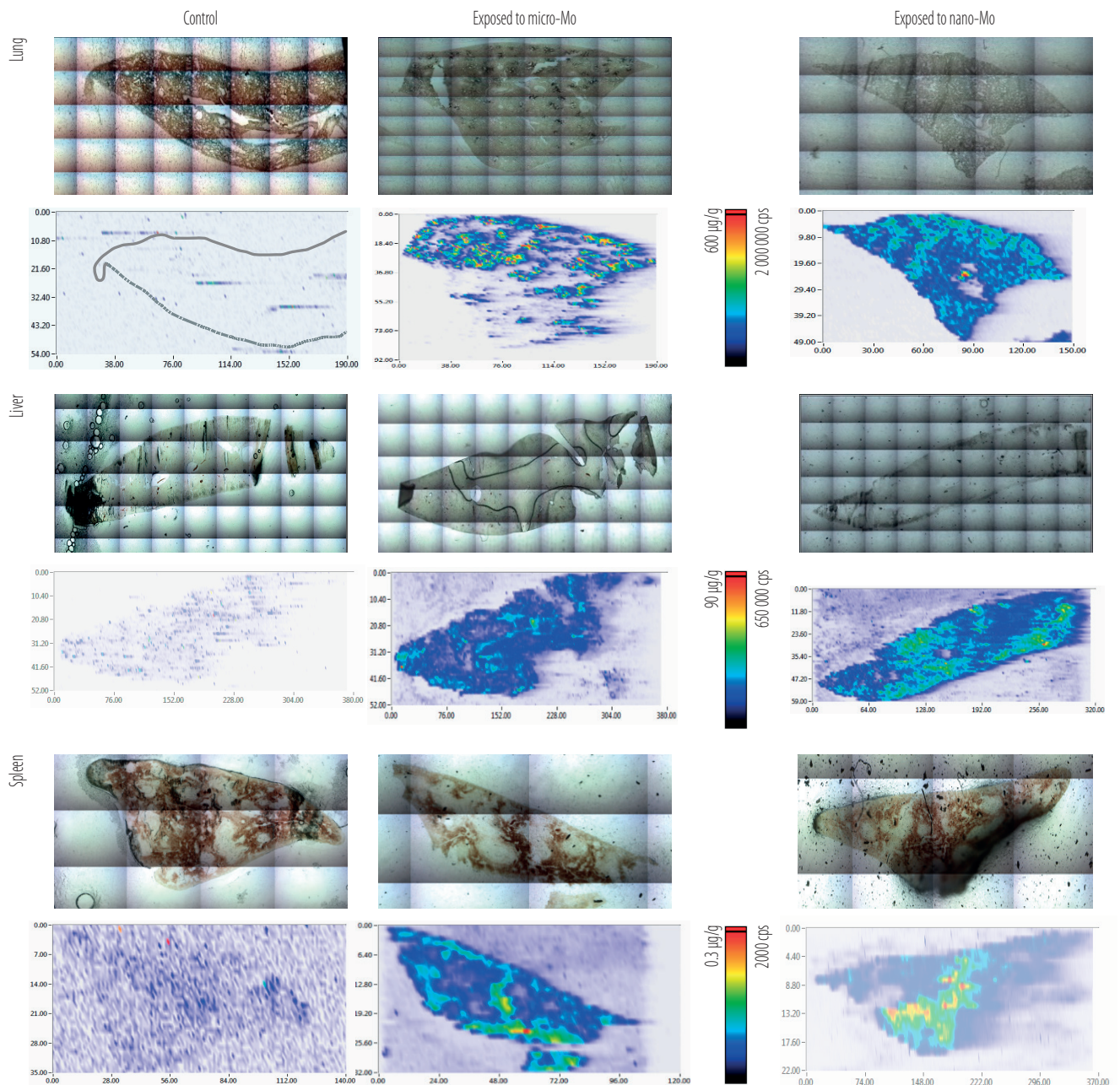
Figure 6. Laser ablation inductively coupled plasma mass spectrometry molybdenum bioimaging ($^{97/95}$Mo ratio) in lung, liver and spleen sections from rats exposed to nano- and microsized molybdenum(IV) disulfide vs. control, normalized to sample size

Analysis of soft tissues

The developed method can be used for practical application to conduct a preliminary verification of Mo concentrations and distribution in selected soft tissues, with a signal intensity ratio of $^{97/95}$Mo (Figure 6).

DISCUSSION

In order to investigate the effect of Mo – in ionic and nano-particle forms – on the tissues, it was necessary to determine elemental spatial distribution and speciation in the tissues. A detailed plan was devised for the devel-

opment of the Mo determination method. Compromise operating conditions for LA and ICP-MS parameters have been set to minimize the operating cost by using the optimization method based on varying one parameter at a time. The first step was to set the appropriate instrumental parameters q. Although labor-consuming, this procedure helped to ensure traceability. It consisted in the optimization of the ICP-MS detection system's parameters, including reaction-gas selection (DRC mode: O and CH_4, and in the KED mode: He), the optimization of the flow rate of the selected reaction gas, the determination of the exclusion parameter RPq, the time setting of data collection, and the selection of the most appropriate standards for the analysis.

To optimize the operating conditions of the LA system, it was necessary to set an appropriate diameter of the laser crater during imaging, as well as the proper distance between the lines, laser energy and laser scanning speed, and also the total sample measuring time. This was to ensure a high quality of the recorded signal on the ICP-MS detector coming from the laser evaporation process. Subsequently, micro- and nanosized Mo distribution on the surface of selected tissue samples was determined and compared with distribution in control tissues. Due to limited research – especially in vitro studies – on the harmful effects of Mo-NPs, an accurate risk assessment of exposure to Mo-NPs is presently not viable.

The online monitoring of different gas flows (He and Ar expressed as l/min, respectively) using the LA system was necessary to optimize the velocity/speed of the gases flowing through the ablation chamber. This is one of the first optimization steps. The rest of the parameters was optimized on selected flows. Next, the study investigated the effect of energy values on the signal intensity of the ^{98}Mo analyte. It is known from previous experience and literature data that the complete vaporization of material obtained from soft tissue samples with a thick-

ness of 20–30 μm is achieved with a laser in the range of 5–10%, corresponding to power density in the range of 1.21–2.41 mJ [20–22]. The study investigated also the effect of scanning speed on analyte signal intensity. Although the optimum scanning speed at the minimum RSD is 0.025 mm/s, this strategy extends the analysis of a single tissue slice to up to several hours. Therefore, the final analysis time will depend on the thickness of the tissue slice. The slower the scanning of the test sample, the better the spatial resolution, and also the stronger the interaction with the slide on which the laser evaporation material is placed. Hence, in order to reduce the duration of laser beam interaction with the slide and its eventual ablation, scanning speed should be increased. The next step was to set the spot size effect on analyte signal intensity. Although the apparatus offers a wide range of options to choose the laser beam size, the mean signal intensity of ^{98}Mo as a function of the laser beam diameter shows that signal intensity at the collimated spot was very low (Figure 2e). A smaller amount of vaporized material that enters the detector may decrease sensitivity – at the same time, however, the image resolution of the analyzed sample increases and so does analysis duration. Therefore, small laser beam diameters should be preferred for analyses of single cells or structures.

After LA optimization, the solid glass standard (NIST612) was used for selecting the appropriate spectrometer measurement mode. This involved evaluating the gas flow rate in the reaction and/or collision chamber and RPq to achieve the best signal response for Mo to the background. This step is important because it eliminates any interferences that may affect the analytical signal. To this end, the difference in signal intensity of the blank (pure gas) and the signal recorded during LA was experimentally verified using the NIST612 reference material. The use of a reaction/collision chamber allows analyte measurement and effective interference removal using CH_4 or O flowing through a DRC or He as the collision gas in the KED mode.

Due to potential spectral interferences from the carrier gas entering the plasma or from multi-atomic ions or isobaric interferences caused by K, ruthenium isotopes present in the matrix, the isotope with the highest abundance ([98]Mo) was chosen to monitor the gas flow rate. Furthermore, it is known that, for the purpose of LA-ICP-MS bioimaging, all intensity data for the elements of interest must be collected simultaneously during a single analysis. This means that the selected elements, in addition to Mo, must also be analyzed under collision or reaction chamber conditions or in a standard mode.

The lack of a common calibration strategy in the LA-ICP-MS technique means that each analysis requires an individual approach [23]. Due to differences in sensitivity drift, the fractionation of elements and/or isotopes, spectral or non-spectral interferences (or other aspects like memory effects), the matrix effect, and the lack of adequate matrix-matched standards [24], a broad range of calibration strategies have been proposed in the scientific literature over the years. Among many possibilities, the most common preparation of the calibration curve involves the use of homogenized tissue with the addition of standard material [2,25,26]. It is known that homogenization affects tissue integrity and sensitivity drift. Compressed tablets of reference materials or synthetic matrices [27] are also fairly common in use, but the use or lack of a binder to pellets divides scientists [28–30]. A direct analysis of a standard solution introduced directly into the ICP-MS can also be applied to an analytics strategy [31–34]. However, limitations due to the difference in sensitivity between external standard analysis and LA require the use of an IS to be corrected [24].

Other calibration strategies include gelatin-based microdroplet standards [35], dried-droplets [36] or spiked agarose gel standards – used by the authors of this paper. The first step was to check for potential Mo presence in a mineralized agarose sample. The raw signal intensity of the element of interest showed some background noise.

The lack of a sufficient starting material (tissue samples) for calibration was clearly a limiting factor here. Moreover, it is worth noting the relatively low cost of agarose. Agarose gels are also non-toxic and easily available for use as calibration standards to determine Mo concentrations in soft tissues. In this study agarose gel standards were prepared. After several weeks, their surface was not smooth and exhibited bulging. Moreover, the spot size of 100 μm partially reduced the relative heterogeneity of the spiked agarose gel effect on LA-ICP-MS. Further work is required to improve the stability of calibration standards. Accordingly, agarose gels were spiked with the Multi-Element CRM Comprehensive Mix B Standard because of the intended use of carbon or sulfur as potential IS correction [21,37]. It is already known that these elements, despite many limitations, are still widely used in correction procedures due to their availability as well as high concentrations in soft tissues. However, the apparent homogeneity in biological matrices is still a challenge. The question of finding an appropriate IS on the market, and determining whether it could be used for analysis or not, is still valid. It is known that CRMs for the elements of interest – with appropriate concentration ranges for soft tissues – are difficult to access, and their preparation is burdened with errors. The specific type of tissue is also a limitation.

The next issue was investigated of Feldman et al. [38] revealed that when applied as IS, ^{13}C improved the RSD for the [63]Cu CRM of the pig liver. However, these authors considered an element that had higher first ionization potential (FIP) than Mo and as such was more susceptible to the matrix effect. Elements with a low FIP – mostly transition elements like Mo (7.09 eV) – can be easily quantified in tissue sections that are 8–30 μm thick [20] because they are not as susceptible to the matrix effect. The FIP for 13C 11.6 eV, its low sensitivity and its known variability in the plasma may substantially alter the ionization efficiency of the analyte [18]. This is related to the occurrence of carbon reaching the ICP in the form

of carbon dioxide. This may modify transport properties and efficiencies. Consequently, they may differ from the analyzed elements which are transported after ablation in the form of particulate matter [21,39]. Moreover, the ionization potential of carbon is significantly higher than that of most transition metals [21]. The viability of ^{13}C as an IS element has been questioned and further research is required on the determination of Mo in soft tissue using LA. Therefore, for the further analysis of soft tissues, the authors of this paper applied an analytical procedure with a tissue section thickness of 20 μm, coupled with an analysis without IS normalization. Because biological tissue is usually non-heterogeneous, and since materials subjected to ablation for many hours show even greater fluctuations and signal drift in ICP-MS than the CRM used for quick analyzes to calculate validation parameters, the experimental strategy was based on an isotopic variant of Mo to correct for instrumental signal drift, matrix effects or analyte losses [20,40,41].

Since the line-by-line ablation mode was used, the final bioimaging resolution was influenced not only by the size of the spots and repetition frequency, but also by scanning speed and spacing between the successive lines. All parameters reflected the above factors. Bioimaging data shows a varying distribution of Mo in the lung, liver and spleen after 7 administrations of nano- and micro-sized MoS$_2$ (every 14 days, with the analysis performed after 90 days) to rats and control rats at a dose of 5 mg MoS$_2$ per kg (PVP). All Mo isotopes were monitored and quantified.

Malinovsky et al. [19] calculated the long-term reproducibility of isotope ratios (in promile, at a 95% confidence level). Their results demonstrate that an external precision changed according to the ratios of $^{100/95}$Mo, $^{98/95}$Mo, $^{97/95}$Mo and $^{96/95}$Mo, and amounted to 0.14‰, 0.08‰, 0.06‰, and 0.04‰, respectively. This will be of particular importance for long-term measurements of tissue sections using the line-by-line mode. During these measurements, gas flow rates, cone contamination, vacuum conditions and other experimental conditions may change over time [21,42]. Thus, for the purpose of analytical measurements, the most suitable ratio was $^{97/95}$Mo, as confirmed by the obtained results. Based on the images of Mo distribution, it can be concluded that repeated intratracheal exposure to both forms of MoS$_2$ leads to its strong accumulation in the lung tissue, with the removal process being very slow. The intensity signal for nano- and micro-sized MoS$_2$ in lung and liver tissues was higher than expected and above the calibration range. The level of nanosized MoS$_2$ was also much higher than in other examined sections, but lower than the level of micro MoS$_2$ in lung tissues. In contrast to lung tissues, the distribution of Mo-NPs was higher in both liver and spleen sections. Mo signal intensity in liver and spleen tissues after 90 days of exposure was slightly higher in the group of animals exposed to Mo-NPs. This may indicate a greater penetration of these particles from the lung tissue into the bloodstream and its further sequestration by the system of mononuclear phagocytes present in the liver and the spleen. According to Chan et al. [43], the incidence of respiratory system lesions in rats increased after the inhalation of molybdenum trioxide. There were dose-dependent relationships. A significant increase in incidence was noted for hyaline degeneration in the nasal epithelium of the exposed rats (10 mg/m^3). Moreover, in the same exposed group, the epithelium lining the base of the epiglottis was found to display squamous metaplasia, unlike in controls. Additionally, the chronic inflammatory reaction was more severe in the rats exposed to 100 mg/m^3 compared to those exposed to 10 or 30 mg/m^3 [43].

There are few publications on Mo concentrations in biological samples. They concern mostly environmental exposure. Stowe et al. [44] took ICP-AES measurements showing that Mo accumulates in higher concentrations in the canine liver (0.23 μg/g). Oymak et al. [45] noticed

the highest Mo levels in livers and kidneys of slaughtered cattle from a local farm in Turkey. The results obtained using ICP-MS showed the following liver and kidney concentrations of Mo: 4.25±0.64 µg Mo/l (liver) and 1.87±0.42 µg Mo/l (kidneys). Nevertheless, some publications that cannot be compared due to different publication times and analytical techniques used. The sample results obtained in this study for single measurements amounted to 124.16 µg Mo/g in the lungs, 183.85 µg Mo/g in the liver and 0.48 µg Mo/g in the spleen for Mo nanoparticles, and to 565.32 µg Mo/g in the lungs, 88.35 µg Mo/g in the liver and 0.25 µg Mo/g in the spleen for the Mo microparticles. Brain tissue levels of Mo in the exposed rats were below the detection limit. Arnaudguilhem et al. [20] present the results of LOD 0.1 µg/g for Mo after normalized results using indium as an IS for thin (8 µm) sections. Feldmann et al. [39] calculated LOD 0.01 µg/g for Mo (5 spots of 200 µm), which was in accordance with the the authors' results. However, it is difficult to compare the levels of endogenous elements after intratracheal instillation with the results obtained after environmental exposure. Furthermore, the study concerned other forms of molybdenum (MoS_2) in rat tissues. Tracheal instillation is commonly used on experimental animals for respiratory toxicity assessments, but significant differences between the techniques used make them difficult to compare [46].

CONCLUSIONS

The LA-ICP-MS technique may be used as an important tool for visualizing the distribution of Mo on the surface of soft tissue samples through quantitative and qualitative elemental mapping.

Author contributions

Research concept: Maciej Stępnik, Beata Janasik
Research methodology: Renata Kuraś, Beata Janasik
Collecting material: Katarzyna Domeradzka-Gajda
Statistical analysis: Renata Kuraś
Interpretation of results: Renata Kuraś, Beata Janasik
References: Renata Kuraś

REFERENCES

1. Theiner S, Kornauth C, Varbanov HP, Galanski, Van Schoonhoven S, Heffeter P, Berger W, Egger AE, Keppler BK. Tumor microenvironment in focus: LA-ICP-MS bioimaging of a preclinical tumor model upon treatment with platinum(IV)-based anticancer agents. Metallomics. 2015 Aug;7(8):1256–1264. https://doi.org/10.1039/c5mt00028a.

2. Costas-Rodríguez M, Van Acker T, Hastuti AAMB, Devisscher L, Van Campenhout S, Van Vlierberghe H, Vanhaecke F. Laser ablation-inductively coupled plasma-mass spectrometry for quantitative mapping of the copper distribution in liver tissue sections from mice with liver disease induced by common bile duct ligation. J Anal At Spectrom. 2017 Jun;32, 1805–1812. https://doi.org/10.1039/C7JA00134G.

3. González de Vega R, Fernández-Sánchez ML, Pisonero J, Eiró N, Vizoso FJ, Sanz-Medel A. Quantitative bioimaging of Ca, Fe, Cu and Zn in breast cancer tissues by LA-ICP-MS. J Anal At Spectrom. 2017 Jan;32,671–677. https://doi.org/10.1039/c6ja00390g.

4. Sajnóg A, Hanć A, Koczorowski R, Makuch K, Barałkiewicz B. Usefulness of laser ablation ICP-MS for analysis of metallic particles released to oral mucosa after insertion of dental

implants. J Trace Elem Med Biol. 2018 Mar;46:46–54. https://doi.org/10.1016/j.jtemb.2017.11.007.

5. Li Q, Wang Z, Mo J, Zhang G, Chen Y, Huang C. Imaging gold nanoparticles in mouse liver by laser ablation inductively coupled plasma mass spectrometry. Sci Rep. 2017 Jun;7(1):2965. https://doi.org/10.1038/s41598-017-03275-x.

6. Cruz-Alonso M, Fernandez B, Navarro A, Junceda S, Astudillo A, Pereiro R. Laser ablation ICP-MS for simultaneous quantitative imaging of iron and ferroportin in hippocampus of human brain tissues with Alzheimer's disease. Talanta. 2019 May;197:413–421. https://doi.org/10.1016/j.talanta.2019.01.056.

7. Hille R, Nishino T, Bittner F. Molybdenum enzymes in higher organisms. Coord Chem Rev. 2011 May;255(9–10):1179–1205. https://doi.org/10.1016/j.ccr.2010.11.034.

8. Zapór L, Cytotoxicity Elicited by Molybdenum Disulphide in Different Size of Particles in Human Airway Cells. Rocz Ochr Śr. 2019 21:794–809.

9. Popławska M, Mikołajczyk U, Bujak-Pietrek S, New sector of employment – A review of data on nanoproduction, research and development in the field of nanotechnology in Poland. Med Pr. 2015 Aug;66(4):575–582. https://doi.org/10.13075/mp.5893.00240.

10. Sobańska Z, Sitarek K, Gromadzińska J, Świercz R, Szparaga M, Domeradzka-Gajda K, Kowalczyk K, Zapór L, Wąsowicz W, Grobelny J, Ranoszek-Soliwoda K, Tomaszewska E, Celichowski G, Roszak J, Stępnik M. Assessment of acute toxicological effects of molybdenum(IV) disulfide nano- and microparticles after single intratracheal administration in rats. Sci Total Environ. 2020 Nov;742:140545. https://doi.org/10.1016/j.scitotenv.2020.140545.

11. Lewis RC, Meeker JD. Biomarkers of exposure to molybdenum and other metals in relation to testosterone among men from the United States National Health and Nutrition Examination Survey 2011–2012. Fertil Steril. 2015 Jan;103(1):172–178. https://doi.org/10.1016/j.fertnstert.2014.09.020.

12. Lewis RC, Johns LE, Meeker JD. Exploratory analysis of the potential relationship between urinary molybdenum and bone mineral density among adult men and women from NHANES 2007–2010. Chemosphere. 2016 Dec;164:677–682. https://doi.org/10.1016/j.chemosphere.2016.08.142.

13. Liu FJ, Dong WY, Zhao H, Shi XH, Zhang YL. Effect of molybdenum on reproductive function of male mice treated with busulfan. Theriogenology. 2019 Mar;126:49–54. https://doi.org/10.1016/j.theriogenology.2018.12.002.

14. Domeradzka-Gajda K, Nocuń M, Roszak J, Janasik B, Quarles CD Jr, Wąsowicz W, et al. A study on the in vitro percutaneous absorption of silver nanoparticles in combination with aluminum chloride, methyl paraben or di-n-butyl phthalate. Toxicol Lett. 2017 Apr;272:38–48. https://doi.org/10.1016/j.toxlet.2017.03.006.

15. Hałatek T, Stanisławska M, Świercz R, Domeradzka-Gajda K, Kuraś R, Wąsowicz W. Clara cells protein, prolactin and transcription factors of protein NF-κB and c-Jun/AP-1 levels in rats inhaled to stainless steel welding dust and its soluble form. Int J Occup Med Environ Health. 2018 Oct;31(5):613–632. https://doi.org/10.13075/ijomeh.1896.01234.

16. Stärk HJ, Wennrich R. A new approach for calibration of laser ablation inductively coupled plasma mass spectrometry using thin layers of spiked agarose gels as references. Anal Bioanal Chem. 2011 Feb;399(6):2211–2217. https://doi.org/10.1007/s00216-010-4413-1.

17. Li Y, Guo W, Hu Z, Jin L, Hu S, Guo Q. Method Development for Direct Multielement Quantification by LA-ICP-MS in Food Samples. J Agric Food Chem. 2019 Jan;67(3):935–942. https://doi.org/10.1021/acs.jafc.8b05479.

18. De Laeter JR, Böhlke JK, De Bièvre P, Hidaka H, Peiser HS, Rosman KJR, Taylor PDP. Atomic weights of the elements. Review 2000 (IUPAC Technical Report), Pure Appl. Chem. 2003; 75(6):683–800. https://doi.org/10.1351/pac200375060683.

19. Malinovsky D, Rodushkin I, Baxter DC, Ingri J, Öhlander B. Molybdenum isotope ratio measurements on geological samples by MC-ICPMS. Int J Mass Spectrom. 2005 Aug;245(1–3):94–107, https://doi.org/10.1016/j.ijms.2005.07.007.

20. Arnaudguilhem C, Larroque M, Sgarbura O, Michau D, Quenet F, Carrère S, Bouyssière B, Mounicou S. Toward

a comprehensive study for multielemental quantitative LA-ICP MS bioimaging in soft tissues. Talanta. 2021 Jan;222: 121537. https://doi.org/10.1016/j.talanta.2020.121537.

21. Limbeck A, Galler P, Bonta M, Bauer G, Nischkauer W, Vanhaecke F. Recent advances in quantitative LA-ICP-MS analysis: challenges and solutions in the life sciences and environmental chemistry. Anal Bioanal Chem. 2015 Sep; 407(22):6593–617. https://doi.org/10.1007/s00216-015-8858-0.

22. Hare DJ, Kysenius K, Paul B, Knauer B, Hutchinson RW, O'Connor C, Fryer F, Hennessey TP, Bush AI, Crouch PJ, Doble PA. Imaging Metals in Brain Tissue by Laser Ablation – Inductively Coupled Plasma – Mass Spectrometry (LA-ICP-MS). J Vis Exp. 2017 Jan;(119):55042. https://doi.org/10.3791/55042.

23. Miliszkiewicz N, Walas S, Tobiasz A. Current approaches to calibration of LA-ICP-MS analysis. J Anal At Spectrom. 2015; 30(2):327–338, https://doi.org/10.1039/C4JA00325J.

24. Lin J, Liu Y, Yang Y, Hu Z. Calibration and correction of LA-ICP-MS and LA-MC-ICP-MS analyses for element contents and isotopic ratios. Solid Earth Sci. 2016 Jun;1(1):5–27. https://doi.org/10.1016/j.sesci.2016.04.002.

25. Egger AE, Theiner S, Kornauth C, Heffeter P, Berger W, Keppler BK, Hartinger CG. Quantitative bioimaging by LA-ICP-MS: a methodological study on the distribution of Pt and Ru in viscera originating from cisplatin- and KP1339-treated mice. Metallomics. 2014 Sep;6(9):1616–25. https://doi.org/10.1039/c4mt00072b.

26. Grijalba N, Legrand A, Holler V, Bouvier-Capely C. A novel calibration strategy based on internal standard-spiked gelatine for quantitative bio-imaging by LA-ICP-MS: application to renal localization and quantification of uranium. Anal Bioanal Chem. 2020 May;412(13):3113–3122. https://doi.org/10.1007/s00216-020-02561-4.

27. Papaslioti EM, Parviainen A, Román Alpiste MJ, Marchesi C, Garrido CJ. Quantification of potentially toxic elements in food material by laser ablation-inductively coupled plasma-mass spectrometry (LA-ICP-MS) via pressed pellets. Food Chem. 2019 Feb;274:726–732. https://doi.org/10.1016/j.foodchem.2018.08.118.

28. Van Heuzen AA, Morsink JBW. Analysis of solids by laser ablation-inductively coupled plasma-mass spectrometry (LA-ICP-MS)—II. Matching with a pressed pellet. Spectrochim Acta Part B At Spectrosc. 1991;46(14):1819–1828, https://doi.org/10.1016/0584-8547(91)80208-K.

29. O'Connor C, Landon MR, Sharp BL. Absorption coefficient modified pressed powders for calibration of laser ablation inductively coupled plasma mass spectrometry. J Anal At Spectrom. 2007;22:273–282. https://doi.org/10.1039/B612512C.

30. Garbe-Schönberg D, Müller S. Nano-particulate pressed powder tablets for LA-ICP-MS. J Anal At Spectrom. 2014 Arp; 29 (6):990–1000. https://doi.org/10.1039/C4JA00007B.

31. Becker JS. Applications of inductively coupled plasma mass spectrometry and laser ablation inductively coupled plasma mass spectrometry in materials science. Spectrochim Acta B At Spectrosc. 2002 Dec;57(12):1805–1820. https://doi.org/10.1016/s0584-8547(02)00213-6.

32. Pickhardt C, Izmer AV, Zoriy MV, Schaumloffel D, Becker JS. On-line isotope dilution in laser ablation inductively coupled plasma mass spectrometry using a microflow nebulizer inserted in the laser ablation chamber ablation chamber. Int J Mass Spectrom. 2006 Feb;248(3):136–141. https://doi.org/10.1016/j.ijms.2005.11.001.

33. Dressler VL, Pozebon D, Mesko MF, Matusch A, Kumtabtim U, Wu B, Sabine Becker J. Biomonitoring of essential and toxic metals in single hair using on-line solution-based calibration in laser ablation inductively coupled plasma mass spectrometry. Talanta. 2010 Oct;82(5):1770–1777. https://doi.org/10.1016/j.talanta.2010.07.065.

34. Hare D, Austin C, Doble P. Quantification strategies for elemental imaging of biological samples using laser ablation-inductively coupled plasma-mass spectrometry. Anal. 2012 Feb; 137(7):1527–1537. https://doi.org/10.1039/C2AN15792F.

35. Schweikert A, Theiner S, Šala M, Vician P, Berger W, Keppler BK, Koellensperger G. Quantification in bioimaging by LA-ICPMS – Evaluation of isotope dilution and standard

addition enabled by micro-droplets. Anal Chim Acta. 2022 Aug 29;1223:340200. https://doi.org/10.1016/j.aca.2022.340200.

36. Bonta M, Hegedus B, Limbeck A. Application of dried-droplets deposited on pre-cut filter paper disks for quantitative LA-ICP-MS imaging of biologically relevant minor and trace elements in tissue samples. Anal Chim Acta. 2016 Feb;908:54–62. https://doi.org/10.1016/j.aca.2015.12.048.

37. Hanć A, Piechalak A, Tomaszewska B, Barałkiewicz D. Laser ablation inductively coupled plasma mass spectrometry in quantitative analysis and imaging of plant's thin sections. Int J Mass Spectrom. 2014;363:16–22. https://doi.org/10.1016/j.ijms.2014.01.020.

38. Feldmann J, Kindness A, Ek P. Laser ablation of soft tissue using a cryogenically cooled ablation. J Anal At Spectrom. 2002 Jul;17:813–818. https://doi.org/10.1039/B201960D.

39. Frick DA, Günther D. Fundamental studies on the ablation behaviour of carbon in LA-ICP-MS with respect to the suitability as internal standard. J Anal At Spectrom. 2012 Jul;27:1294–1303. https://doi.org/10.1039/C2JA30072A.

40. Douglas DN, O'Reilly J, O'Connor C, Sharp BL, Goenaga-Infante H. Quantitation of the Fe spatial distribution in biological tissue by online double isotope dilution analysis with LA-ICP-MS: a strategy for estimating measurement uncertainty. J Anal At Spectrom. 2016;31:270. https://doi.org/10.1039/C5JA00351B.

41. Moraleja I, Mena ML, Lázaro A, Neumann B, Tejedor A, Jakubowski N, Gómez-Gómez MM, Esteban-Fernández D. An approach for quantification of platinum distribution in tissues by LA-ICPMS imaging using isotope dilution analysis. Talanta. 2018 Feb;178:166–171. https://doi.org/10.1016/j. talanta.2017.09.031.

42. Koch J, Günther D. Review of the state-of-the-art of laser ablation inductively coupled plasma mass spectrometry. Appl Spectrosc. 2011 May;65(5):155–162. https://doi.org/10.1366/11-06255.

43. Chan PC, Herbert RA, Roycroft JH, Haseman JK, Grumbein SL, Miller RA, Chou BJ. Lung tumor induction by inhalation exposure to molybdenum trioxide in rats and mice. Toxicol Sci. 1998 Sep;45(1):58–65. https://doi.org/10.1006/toxs.1998.2497.

44. Stowe HD, Braselton WE, Slanker M, Kaneene JB. Multielement assays of canine serum, liver, and kidney by inductively coupled argon plasma emission spectroscopy. Am J Vet Res. 1986 Apr;47(4):822–827.

45. Oymak T, Ulusoy Hİ, Hastaoglu E, Yılmaz V, Yıldırım Ş. Some Heavy Metal Contents of Various Slaughtered Cattle Tissues in Sivas-Turkey. JOTCSA 2017;4(3):721–728. https://doi.org/10.18596/jotcsa.292601.

46. Hasegawa-Baba Y, Kubota H, Takata A, Miyagawa M. Intratracheal instillation methods and the distribution of administered material in the lung of the rat. J Toxicol Pathol. 2014 Oct;27(3–4):197–204. https://doi.org/10.1293/tox.2014-0022.